

The Star Formation History and Mass Function of the Double Cluster h and Chi Persei

Catherine L. Slesnick¹, Lynne A. Hillenbrand¹

Dept. of Astronomy, MS105-24, California Institute of Technology, Pasadena, CA 91125

`cls@astro.caltech.edu, lah@astro.caltech.edu`

and

Philip Massey¹

Lowell Observatory, 1400 W. Mars Hill Road, Flagstaff, AZ 86001

`Phil.Massey@lowell.edu`

ABSTRACT

The h and χ Per “double cluster” is examined using wide-field ($0.98^\circ \times 0.98^\circ$) CCD *UBV* imaging supplemented by optical spectra of several hundred of the brightest stars. Restricting our analysis to near the cluster nuclei, we find identical reddenings ($E(B - V) = 0.56 \pm 0.01$), distance moduli (11.85 ± 0.05), and ages (12.8 ± 1.0 Myr) for the two clusters. In addition, we find an IMF slope for each of the cluster nuclei that is quite normal for high-mass stars, $\Gamma = -1.3 \pm 0.2$, indistinguishable from a Salpeter value. We derive masses of $3700 M_\odot$ (h) and $2800 M_\odot$ (χ) integrating the PDMF from 1 to $120 M_\odot$. There is evidence of mild mass segregation within the cluster cores. Our data are consistent with the stars having formed at a single epoch; claims to the contrary are very likely due to the inclusion of the substantial population of early-type stars located at similar distances in the Perseus spiral arm, in addition to contamination by G and K giants at various distances. We discuss the uniqueness of the double cluster, citing other examples of such structures in the literature, but concluding that the nearly identical nature of the two cluster cores is unusual. We fail to settle the long-standing controversy regarding whether or not the double cluster is the

¹Visiting astronomer, Kitt Peak National Observatory, a division of the National Optical Astronomy Observatory, which is operated by the Association of Universities for Research in Astronomy, Inc., under cooperative agreement with the National Science Foundation.

core of the Per OB1 association, and argue that this may be unanswerable with current techniques. We also emphasize the need for further work on the pre-main sequence population of this nearby and highly interesting region.

Subject headings: stars: early-type – open clusters and associations: individual (NGC869, NGC 884)–stars: luminosity function, mass function

1. Introduction

The “double cluster” η and χ Persei (hereafter η/χ Per; also known as NGC 869 and NGC 884, respectively) is among the brightest, densest, and closest of the open clusters containing moderately massive stars. The double cluster has been studied extensively over the last century (e.g. Oosterhoff 1937; Bidelman 1943; Wildey 1964; Schild 1965, 1967; Crawford, Glaspey, & Perry 1970; Vogt 1971; Tapia et al. 1984; Waelkens et al. 1990) with resulting mean reddenings of $E(B - V) = 0.5-0.6$, and distance moduli in the range 11.4-12.0 mag (1.9-2.5 kpc). The clusters contain several tens of Be stars (e.g. Slettebak 1968; Bidelman 1947a; see also Keller et al. 2001). Wildey’s (1964) HR diagrams suggested several distinct episodes of star formation (7 Myr, 17 Myr, and 60 Myr), which would imply a spread of >50 Myr in the formation times of OB stars in a single (double) cluster! This age spread is larger than that claimed for any other well-studied open cluster, and is one of the primary motivations of the present investigation.

Most previous work on η/χ Per has used photographic or single-channel photoelectric photometry with little emphasis on spectroscopy. Several very recent papers have used CCDs but consisted of photometric analysis only ($UBVI/H\alpha$, Keller et al. 2001; $ubvy/\beta$, Marco & Bernabeu 2001). Distance moduli in the range 11.6-11.8 mag and ages of 10-20 Myr have been found, with Marco & Bernabeu (2001) arguing (like Wildey 1964) for three distinct episodes of star formation, while Keller et al. (2001) find instead a single age. There is significant disagreement between various authors as to whether the reddenings, distances, and ages of the two clusters are identical or substantially (30-50%) different. It is especially important to understand in detail the star formation history of η/χ Per as these clusters are widely used from professional review papers to basic introductory astronomy textbooks to illustrate upper main sequence stellar evolution.

Our modern study of η/χ Per consists of wide-field CCD UBV photometry for 4528 stars and blue optical spectroscopy for 196 of the stars presumed to be the most massive (i.e., the brightest blue and red stars). Our main goals are to re-determine the distance, age, and age spread in the double clusters, and to explore for the first time the mass function and the

evidence for mass segregation. In section 2 we describe our data acquisition, reduction, and preliminary photometric and spectroscopic analysis. In section 3 we present color magnitude diagrams, an assessment of field star contamination, a derivation of reddening and distance, and a Hertzsprung-Russell (HR) diagram along with discussion of stellar age and mass distributions. Section 4 contains our discussion of the uniqueness of this double cluster, and the relationship between it and the surrounding region. In Section 5 we summarize our results.

2. Observations and Data Reduction

2.1. Photometry

UBV photometry was obtained from observations with the 0.9-m telescope at Kitt Peak National Observatory using the Mosaic CCD camera (0.43 arcsec/pixel) on 1999 Feb 3. Conditions were photometric with ~ 1.3 arcsec seeing. The Mosaic camera consists of 8 individual SITe 2048×4096 CCD chips arranged in 2 rows of 4 to produce a final image equivalent to 8192×8192 pixel² (0.98×0.98 deg²) but with modest (35 to 50 pixel) gaps. Our imaging data set contains short (0.5 sec in *V* and *B*, and 2 sec in *U*), medium (2 sec in *V* and *B*, and 10 sec in *U*), and long (100 sec in *V* and *B*, and 300 sec in *U*) integrations, each consisting of 5 dithered exposures which were combined to fill in gaps between the 8 chips. The exceptions to this pattern are the short exposures which were not dithered, and the medium *B* exposure which only had 4 dithers instead of 5. Many Landolt (1992) standards were observed for the purposes of transformation to the *UBV* system.

For the basic reductions we followed the precepts of Valdes (1998), using the IRAF “mscred” package. With bright twilight flats we were able to flatten the data to $< 1\%$ in terms of large-scale gradients. As the plate scale changes significantly over the field of view, care must be taken to geometrically correct the data to a uniform sampling for the premise of aperture photometry to work; this transformation was made using a sinc interpolation in order to come close to preserving the Poisson noise characteristics.

A common but hitherto untested practice when working with Mosaic data is to combine each set of ditherings into a single “stacked” image for photometry. However, each chip has its own spectral response and hence, color term. Since any given star may be the average of multiple dithered exposures and may appear on up to 4 of the CCDs, we were driven to wonder to what degree of accuracy one could do photometry using the final combined images. We thus performed both aperture photometry and point-spread-function (PSF) fitting photometry separately on both the stacked images (9 total = 3 colors \times 3 integration

times) and the individual CCD frames (247 total = 8 chips \times 1,4, or 5 ditherings \times 3 colors \times 3 integration times). Color terms were determined for each of the 8 chips individually. We retained the median value in each filter for the stacked images. On the whole, color-term variations were most significant at U . By adopting a single color-term for the stacked images we expect to make systematic errors in V by an average of 0.012 magnitudes over a color range in $(B - V)$ of 1. The maximal chip to chip difference is 0.032 mag in V . The B band gave similar residuals with a full range of 0.038 per one magnitude range $(B - V)$. In U band the chip-to-chip offsets were considerably larger, yielding typical variations of 0.038 mag over a range of 1 mag in $(U - B)$ and a maximal difference of 0.11 mag.

We found that PSF-photometry of the stacked images produces errors of $> 5\%$, independent of magnitude, suggesting that these errors are not dominated by photon noise. The scatter for the individual frame PSF photometry was also magnitude-independent and gave errors of $\sim 3\%$ when compared to aperture photometry of single isolated stars. We could see by visual inspection that there were significant variations in the PSF even across a single chip, despite the relatively slow (f/7.5) beam.² Accordingly we choose to rely upon aperture photometry alone, sacrificing the potential advantage of PSF-fitting for any crowded stars. Fortunately h/ χ Per is relatively sparse. Over the entire imaged area, the mean stellar density to $V = 15$ mag is 0.7 stars arcmin⁻²; in the center of the clusters, it is still a modest 2.2 and 1.7 stars arcmin⁻² for h and χ , respectively.

Our standard and program stars were each measured with the same large aperture (10 pixel radius = 8.6 arcsec diameter). The standard star data were then used to produce transformations between the instrumental and standard system, The extinction values we found were typical of Kitt Peak, and our fits had small (< 0.02 mag) residuals.

Because our frames went much deeper than any program stars of interest (thanks to the long-exposure frames) we had the luxury of retaining only the very best data for the subsequent analysis. After merging the data for the three sets of exposures times, we kept only those stars for which the instrumental errors (due to photon-statistics and read-noise) were less than 0.01 mag in U , B , and V . This eliminated roughly 96% of the stars we had measured, and is equivalent to simply imposing a magnitude cut-off on the data. Thus while our catalog does not go as deep as other recent efforts (cf. Keller et al 2001) our photometric errors are quite small and we purposefully chose to truncate our catalog once field contamination became extreme.

Table 1 contains our catalog of h/ χ Per stars, ordered by decreasing brightness. We have

²Subsequent to these data being obtained, the corrector in the 0.9-m was realigned, leading to improved behavior of the PSF.

merged the photometry for the three sets of exposures, weighting inversely by the square of the photometric uncertainty. Our final source list contains three-filter photometry for 4528 stars down to $V \sim 16$ mag. We can estimate our completeness from the histograms of the number of stars per 0.25 mag bin shown in Fig. 1 and find completeness of our catalog to $U \sim 16.2$, $B \sim 16.0$, $V \sim 15.0$.

How well does our photometry agree with earlier studies? In Fig. 2 we compare our work with a subset of Wildey’s (1964) photoelectric and photographic work, concentrating primarily on the brighter stars and those for which we have spectral types. We see that his photometry and ours agree extremely well given the differences in equipment. We find differences (in the sense of our data minus Wildey’s) with his photographic data of $(\Delta V)_{avg} = 0.097 \pm 0.027$, $[\Delta(B - V)]_{avg} = -0.044 \pm 0.009$, and $[\Delta(U - B)]_{avg} = -0.069 \pm 0.036$ computed from a comparison of 300 stars. Comparing our photometry to 24 of Wildey’s photoelectrically observed stars we find even smaller average offsets of $(\Delta V)_{avg} = 0.020 \pm 0.022$, $[\Delta(B - V)]_{avg} = -0.014 \pm 0.026$, and $[\Delta(U - B)]_{avg} = 0.017 \pm 0.012$. The scatter is larger and asymmetrical in the V comparison (see Fig. 2), in the sense one would expect if Wildey’s work occasionally had faint stars in the sky determination. In a similar comparison with Wildey’s photographic study, Keller et al. (2001) quote average differences of $(\Delta V)_{avg} = 0.16$, $[\Delta(B - V)]_{avg} = -0.03$, and $[\Delta(U - B)]_{avg} = 0.00$, attributing the offset with respect to Wildey’s V -band photometry to crowding effects. We have matched our data to that of Keller et al. (2001) for stars which are not known from the literature to be variable and for which we have identified Oosterhoff (1937) numbers (again, our cross-identification is not complete), and find average offsets of $(\Delta V)_{avg} = -0.019 \pm 0.008$, $[\Delta(B - V)]_{avg} = 0.001 \pm 0.026$, and $[\Delta(U - B)]_{avg} = -0.048 \pm 0.014$ computed from 55, 31 and 49 stars, respectively. The generally good agreement between all three studies is a testament to Wildey’s painstaking accuracy in centering stars with a photoelectric photometer, and also supports the validity of our reduction procedure and transformation to the standard photometric system.

2.2. Spectroscopy

Several hundred spectral types complement our photometric database. For hot stars, spectral data are needed to obtain accurate effective temperatures and consequently accurate extinction estimates and bolometric corrections (Massey 1998a, 1998b), all necessary for locating a star in the HR diagram. We selected stars for spectroscopy based on their brightness and colors. Since we did not yet have our own CCD photometry at the time the spectroscopic program was begun we worked largely from the Wildey (1964) photometry; this introduces a bias towards blue stars closer to the cluster nuclei. Later spectroscopic

runs incorporated a wider range of magnitude and color selection, probing down as far as mid-A spectral types in an unrealized attempt to identify possible pre-main sequence stars amidst substantial field star contamination. In the lower-left panel of Fig. 4 we show the spatial distribution of the spectroscopic sample compared to the entire photometric sample; in the upper-left panel we show the loci of the spectroscopic sample in the color-magnitude plane. Of the brightest 50 stars, we have spectral types for 49, regardless of location in our field. Fainter than that the spectroscopic campaign was concentrated in the cluster cores.

Spectroscopic data were taken at several NOAO telescopes. We employed the WIYN 3.5-m telescope and the Hydra multi-fiber positioner to feed a bench-mounted spectrograph (1993 Dec and 1994 Oct), the KPNO 4-m telescope and the RC spectrograph in multi-slit mode (1994 Nov and 1999 Aug), the KPNO 2.1-m telescope and GoldCam with a single slit (1994 Sept), and the Coude Feed (1999 July and Nov). For most of the spectra the spectral range is $\sim \lambda\lambda 3900\text{--}4700 \text{ \AA}$ at a resolution of $\sim 1.5 \text{ \AA}$. Higher resolution was obtained with the Coude Feed data, which were taken in multiple wavelength settings. One-dimensional spectra were extracted from the two-dimensional images using the slit and multi-fiber reduction packages within IRAF. Signal-to-noise ranged from $\sim 20\text{--}150$ with nearly all spectra classifiable. Fig. 3 shows three spectra taken at the KPNO 2.1-m telescope with GoldCam which illustrate the effects of temperature on B-type supergiants.

We present in Table 1 new spectral types for 196 stars, many of which result from several different observations of the same object. In classifying the spectra we followed the guidelines of Walborn & Fitzpatrick (1990), Jaschek & Jaschek (1987), and Jacoby, Hunter, & Christian (1984). All stars were classified by a minimum of two of the authors, both independently and collaboratively. Spectral types assigned by us were also compared to those in the literature where available, and we cite these older spectral types as well. As emphasized in the introduction, spectroscopic efforts have lagged behind photometric studies of this region. Johnson & Morgan (1955), Schild (1965, 1967), and Slettebak (1968) have made the most systematic efforts in this regard, and in general our spectral types agree very well with theirs.

The most luminous stars we identify in the vicinity of h/χ Per are M, A, and B supergiants. There is a lone O-type star, HD 14434 (O6.5V). As we discuss below, this star is likely not a member of the double cluster, but appears to be a younger field star interloper at approximately the same distance. The remainder of the spectra are slightly evolved B-type giants and B- and A-type dwarfs. We identify ten Be stars, two of which were previously unknown. Six out of seven stars which were classified photometrically as Be stars by Keller et al. (2001) using $(V - H\alpha)$ colors and which we have our own spectra for, do in fact prove to be emission line objects. Since none of our spectra extend as far redwards as $H\alpha$, emission

seen by us is usually in $H\beta$ which tends to be weaker than $H\alpha$ emission by $\approx 1/3$.

3. Analysis

Our analysis includes discussion of color-magnitude diagrams, assessment of field star contamination, derivation of cluster reddening and distance, and construction of HR diagrams. We then discuss stellar ages and masses as inferred from the HR diagrams, and the distribution of ages and masses within the clusters.

We expect that stars near the cluster cores predominantly will be members, while stars further afield will be a mixture of both members and non-members. We constructed a contour plot of the spatial distribution of stars within our field, and found that the stellar densities were enhanced by 2σ at identical radii of 7 arcminutes from each of the cluster cores; we will use this radial criterion when describing stars near the nuclei. We also determined accurate centers for the two cores ($\alpha_{2000}=2:19:22.2$, $\delta_{2000}=+57:09:00$ for h Per , and $\alpha_{2000}=2:22:12.0$, $\delta_{2000}=+57:07:12$ for χ Per) by examining mass and number density contours.

Tables 2a & 2b contain derived quantities for stars near to (≤ 7 arcmin) and further away from the cluster centers, respectively. We have limited these tables to those stars which we included in determining the PDMF (see section 3.4.4).

3.1. Color-Magnitude Diagrams and the Influence of Field Stars

In Figure 4 we show the color-magnitude diagram (CMD) for (1) all of the stars over the full 0.98×0.98 deg² covered in our CCD images (left panels), and (2) only the stars within 7 arcmin of each of the two cluster nuclei. The influence of field stars can be seen in the upper left panel of this figure, notably between $0.5 < (B - V) < 1.0$ and $10 < V < 16$. For the h and χ cluster nuclei in the upper right panel, field star contamination is less severe, but still present. The close match between the two CMDs suggests that there are no substantial differences in reddening, distance or age between the two clusters, a conclusion we explore in greater depth below.

To further assess the field star contamination we use the density of stars in the color-magnitude diagrams (i.e., a ‘‘Hess’’ diagram), as shown in Figure 5 for both V vs. $(B - V)$ and V vs. $(U - B)$. We define the ‘‘cluster region’’ as above, while the ‘‘field stars’’ region is arbitrarily taken as the northern 0.25 deg and southern 0.15 deg of our CCD imaging area. Hess diagrams produced for this total area of 0.4 deg² were scaled up to the full area of the CCD survey (shown as red contours in the upper panels of Figure 5) and subtracted from

the Hess diagram constructed over the full imaging area. The result of this subtraction is shown in the lower panels, with the resulting V vs. $(B - V)$ and V vs. $(U - B)$ diagrams displaying a much tighter color-magnitude sequence than the full area.

3.2. Reddening

For each star with a spectral type we compute the color excess using the spectral type-intrinsic color relations of FitzGerald (1970). The average value of color excess for 123 stars with well determined spectral types is $E(B - V) = 0.55$, with a 1σ variation of 0.1. For the 56 stars near the core of h Per we find an average $E(B - V) = 0.57$, with a 1σ variation of 0.08. Similarly for 40 stars near the core of χ Per we find an average of 0.53 ($1\sigma=0.08$). The median values are 0.56 mag, 0.57 mag, and 0.55 mag for the three samples, respectively. We conclude that the reddening is indistinguishable for the two clusters and, further, infer that the reddening is entirely due to line of sight extinction to the Perseus spiral arm with intracluster reddening essentially zero. This is consistent with a 3σ upper limit on ^{13}CO emission (Hillenbrand & Carpenter; unpublished FCRAO data) corresponding to essentially no gas ($N(^{13}\text{CO}) < 2.1 \times 10^{15} \text{ cm}^{-2}$) or dust ($A_V < 1.4$ mag) within the clusters.

In dereddening the photometry, we assume the standard 3.1 ratio of total-to-selective absorption. For other stars without spectral types, color excesses were determined using the “ Q method”, where applicable: following Massey (1998a), for stars with $B - V < 0.5$, we compute $(B - V)_o = -0.0186 + 0.3218 \times Q$, where $Q = (U - B) - 0.72 \times (B - V)$ is a reddening-independent index. The relation between $(B - V)_o$ and Q was derived by fitting the intrinsic color relationships of FitzGerald (1970) for main-sequence stars, but the relationship can be used for supergiants and giants. For stars without spectral types, we adopt the median $E(B - V)$ of 0.56.

3.3. Distance

We determine the distances to the clusters using two methods: spectroscopic parallax and “main-sequence” fitting. We discuss these two approaches separately and then comment on their respective merits.

3.3.1. Spectroscopic Parallax

For each star with a spectral type we compute the distance modulus by first dereddening the data using the intrinsic colors of FitzGerald (1970), and then finding $V_o - M_V$. We have adopted the spectral type- M_V calibration of Conti (1988) for our one O-type star and that of Humphreys & McElroy (1984) for everything else (B-type through M-type), interpolating values for spectral types not explicitly present in these tables when needed. For the stars with well defined spectral types we find a distance modulus of 12.5 ± 0.5 mag when we restrict ourselves to the objects within the cluster cores.

This method works relatively well for very young (< 3 Myr) clusters (see Massey, Johnson, & DeGioia-Eastwood 1995) where there is a fairly gradual change of M_V with spectral type among the O-type stars (Conti 1983), about 1.4 mags from O3 V to O9.5 V. For a 10-20 Myr old cluster, the only stars left on the main-sequence are B-type stars, and there M_V changes by 3 magnitudes over the spectral range B0 V to B8 V. In addition, the luminosity criteria for B-type stars are rather subtle compared to that of the O-type stars; for the former it depends upon the absolute strengths of the Si lines (which are also temperature dependent), while for O-type stars it depends primarily on He II $\lambda 4686$ being in emission or absorption.

We did examine the spectroscopic parallaxes as a function of luminosity class. Although the median distance moduli for luminosity class V, III, and I stars are about the same, in each case there is a large spread in the values which we attribute to errors in placing the stars into the correct luminosity class. Due to the subtleties involved, some misclassifications are inevitable, and in addition membership issues may also come into play. More significantly, stars which are really luminosity class IV and hence follow their own (and presently undetermined) spectral type- M_V calibration are placed at present into either luminosity class III or class V. The same holds for luminosity class II stars which often wind up being called either class I or class III due to lack of observational distinction between the classes.

Using only the brightest stars ($V < 10.5$) we find a distance modulus of 11.95 ± 0.2 , in substantial agreement with what we find below. These brighter stars are among the earliest types, yet include many supergiants whose intrinsic luminosity has a large scatter. However, the strength of the Si lines make spectral classification more certain in classifying hot giant and supergiant stars. Therefore, spectral types and luminosity classes will be better determined for these bright stars.

3.3.2. Main-sequence Fitting

We can also use “main-sequence fitting” to determine the average distance of the lower-mass, unevolved stars in our sample. Given the approximate age of the clusters (13 Myr, as will be discussed in section 3.4.3) this is not a trivial exercise and must be done using post- and pre-main sequence evolutionary tracks combined. Although many renditions of the “observed” main sequence exist (e.g. Balona & Shobbrook 1984; Balona & Feast 1975; Morton & Adams 1968; Blaauw, 1964), any relationship between M_V and $(B - V)_o$ derived for stars in the solar vicinity necessarily contains only the mean M_V value characteristic of the typical age in the solar neighborhood of stars with that $(B - V)_o$. For example, the M_V ’s at the bluest values of $(B - V)_o$ represent ages of only 1-2 Myr while the M_V ’s around $(B - V)_o=0$ represent ages of a few hundred Myr and the M_V ’s around the $(B - V)_o$ color of the Sun represent ages of more than a Gyr. In h/ χ Per, plotting the de-reddened cluster data points against an “observed” main sequence results in the “main sequence” being too blue/faint at the bluest colors (since the h/ χ Per stars are evolved away from the zero-age main sequence) and too bright/red at the redder colors (since the h/ χ Per stars are younger than the mean age of stars in the solar vicinity and, hence, not yet far enough evolved from the empirical “zero-age” main sequence to the position where stars having the mean age of the solar neighborhood would lie). Comparison to a theoretical “zero-age main sequence” involves similar concepts.

“Main sequence fitting” therefore must be done when trying to fit more evolved clusters using theoretical isochrones. We use the solar-metallicity ($Z = 0.02$) post-zero-age main sequence tracks and isochrones of Schaller et al. (1992), which include convective overshoot and standard mass-loss rates. In addition, we use the pre-main sequence tracks and isochrones from the same group, published in Bernasconi (1996). We transform these tracks and isochrones from M_{bol} and $\log T_{eff}$ to V_o and $(B - V)_o$ using the same, though inverted, relationships that we use later to transform our data from the observational V_o and $(B - V)_o$ plane to the theoretical M_{bol} and $\log T_{eff}$ plane (see Section 3.4). Figure 6 is a CMD of our dereddened photometry where we have used the isochrones to determine the distance. As in Figure 4, blue and red points represent stars which are spatially located within 7 arcmin from the centers of h Per and χ Per, respectively.

The “main sequence fitting” procedure is complicated by the fact that in order to obtain a best fit distance modulus from theoretical isochrones an approximate age must be assumed. We explored isochrones spanning a wide range in age (1-50 Myr) and found that the isochrone shape matches the cluster data best for both post- and pre-main sequence tracks in the 10-20 Myr range. Using this information, we find a best fitting distance modulus of 11.85 ± 0.05 mag corresponding to a distance of 2344^{+55}_{-53} pc, where we have estimated both the fit and

uncertainty by eye in matching the models to the data.

Good agreement is seen between the post-zero-age main sequence turnoff at $(B - V)_o \leq -0.22$ and pre-zero-age main sequence turn-on at $(B - V)_o \geq 0.1$ using the Schaller et al. (1992) and Bernasconi (1996) calculations *when transformed using our equations relating T_{eff} with $(B - V)_o$ colors and bolometric corrections*. Using transformations to the color-magnitude plane supplied directly by the authors (which rely upon the Schmidt-Kaler (1982) relationships) does not produce a match between the theory and the data for any isochrone. However, using our transformation equations (derived primarily from stellar atmosphere models) we find extremely good agreement between our dereddened data and the stellar evolutionary isochrones. As can be seen in Fig. 6, at an age of 10-15 Myr, we expect to see significant contributions from the pre-main-sequence population at $M_v \sim 2$. However, due the large amount of field star contamination in this region, the extent of this effect in our sample is difficult to determine.

Fig. 6 effectively puts to rest any question as to whether or not h and χ Per are at two different distances rather than one. This result is supported by similar conclusions found by Keller et al. (2001).

Why are the distance moduli derived from spectroscopic parallax (12.5 mag) and photometric parallax (11.85 mag) so different? The slightly evolved state of the main-sequence stars that dominate our spectroscopic sample should actually lead to our computing too *small* a spectroscopic distance modulus rather than too great a number. We believe there is need for good recalibration of the spectral-type to M_V relation using a variety of clusters and associations with good distance moduli determined from spectroscopic parallax of O-type stars, as well as direct determinations via modern trigonometric parallaxes.

3.4. The Hertzsprung-Russell Diagram

3.4.1. Transformations

The effective temperatures and bolometric corrections of our stars were determined using photometry and spectral types, if available, or photometry alone, otherwise, in order to place the stars in the HR diagram. For those stars with spectral types we adopt the calibration of Kilian (1992) for the early B dwarfs and giants, and that of Humphreys & McElroy (1983) for all other stars. When spectral types were not available, empirically derived relationships were used to transform photometry to $\log T_{\text{eff}}$ and M_{bol} . Effective temperatures were derived for bluest stars ($Q < -0.6$) using the Q - $\log T_{\text{eff}}$ relationships given by Massey, Waterhouse, & DeGioia-Eastwood (2000), namely:

$$\log T_{\text{eff}} = -0.9894 - 22.7674 \times Q - 33.0964 \times Q^2 - 16.19307 \times Q^3 \quad \text{[I]}$$

$$\log T_{\text{eff}} = 5.2618 + 3.4200 \times Q + 2.93489 \times Q^2 \quad \text{[III]}$$

$$\log T_{\text{eff}} = 4.2622 + 0.6452 \times Q + 1.09174 \times Q^2 \quad \text{[V]}$$

For stars that failed to meet this criterion, we used empirical fits to a combination of “observed” (Flower 1996) and theoretical (Kurucz 1992) colors and effective temperatures. The former must be used with some caution as there is no reddening correction for what are presumed to be nearby stars. We found:

$$\begin{aligned} \log T_{\text{eff}} = & 3.9889 - 0.7950 \times (B - V)_o + 2.1269 \times (B - V)_o^2 - 3.9330 \times (B - V)_o^3 + \\ & 3.5860 \times (B - V)_o^4 - 1.5531 \times (B - V)_o^5 + 0.2544 \times (B - V)_o^6 \end{aligned}$$

The bolometric correction as a function of effective temperature is that derived by Hillenbrand (1997) for dwarf stars but modified to account for the presence of M supergiants in our sample by adopting the values in Humphreys & McElroy (1984). Thus

$$\text{BC} = -8.58 + 8.4647 \times \log T_{\text{eff}} - 1.6125 \times (\log T_{\text{eff}})^2 \quad [\log T_{\text{eff}} > 4.1]$$

$$\text{BC} = -312.90 + 161.466 \times \log T_{\text{eff}} - 20.827 \times (\log T_{\text{eff}})^2 \quad [4.1 > T_{\text{eff}} > 3.83]$$

$$\text{BC} = -346.82 + 182.396 \times \log T_{\text{eff}} - 23.981 \times (\log T_{\text{eff}})^2 \quad [3.83 > T_{\text{eff}} > 3.55]$$

$$\text{BC} = -2854.91 + 1590.11 \times \log T_{\text{eff}} - 221.51 \times (\log T_{\text{eff}})^2 \quad [3.55 > T_{\text{eff}}]$$

3.4.2. The HR Diagram

Figure 7 is the resulting HR diagram. Post-zero-age main sequence evolutionary tracks and isochrones are transformed as above from the $\log T_{\text{eff}}$ and M_{bol} values calculated by Schaller et al. (1992). All stars with MK spectral classifications of luminosity class I or III, and stars earlier than B5 with luminosity class IV or V were placed spectroscopically (larger, filled in circles) while most other stars were placed photometrically (open circles). The left panel shows data for the entire imaging area while the right panel contains only stars within 7 arcmin of the cluster nuclei. No corrections for field star contamination have been applied and, as was the case for the color-magnitude diagrams (Fig. 5), the HR diagrams for the central regions of the clusters contain significantly less field star contamination, especially

above the main sequence. Note the presence of the O-type star HD 14434 on the left panel of Fig. 7. It is highly discrepant in age, and, combined with its location outside the cores of the clusters, we dismiss this star as field star.

From these HR diagrams we immediately see that the h/ χ Per clusters are slightly evolved from the zero-age main sequence and that the most massive stars are only $\approx 20 - 30M_{\odot}$. The data extend down to about $3M_{\odot}$ before field star contamination becomes substantial.

3.4.3. *Stellar Ages and the Age Distribution*

For finding ages, we use our dereddened CMD data (Fig. 6) with a grid of isochrones computed at intervals of 0.1 Myr from 5-30 Myr.³ We restrict ourselves only to the most luminous stars ($M_V < -3$), as it is only near and above the turn-off that there is good age information. We filter out the obvious foreground contaminants e.g., $(B - V)_o > -0.2$ for $-3 > M_V > -5$. We cannot use the RSGs for our age determinations, unfortunately, since the evolutionary tracks do not actually extend that far to the red; we will note, though, that the location of the RSGs in the CMD are consistent with the ages we derive were we to extrapolate the isochrones. For each of our clusters we find essentially identical ages: 12.8 Myr and 12.9 Myr for h and χ respectively. The formal errors of the mean on these determinations are 1 Myr, and the scatter is ~ 5 Myr; the latter is dominated by observational errors at the <0.01 mag level.

We do not find evidence for multiple distinct episodes of star formation despite the remarkable similarities between our dereddened CMD and Wildey’s (1964). We believe the difference in interpretation occurs because Wildey in his original analysis did not consider the possibility of field star contamination from G and K giants seen to large distances through the Galaxy. It is clear from the right panel of Figure 7 that when just the cluster nuclei are considered any apparent branching in the HR diagram is significantly diminished. We do find several high-mass stars with uncharacteristically young ages as compared to the rest of the cluster. However, in most cases these stars are either not in the central regions of the

³We use the CMD rather than the HRD data to determine ages in order to avoid the quantization problem introduced by spectral types. The ages are very sensitive to $\log T_{\text{eff}}$ (or $(B - V)_o$), and thus this quantization would introduce a spurious age spread. The spectral types *have* been employed in the CMD in order to derive $E(B - V)$. In a subsequent section we *will* use the HRD to derive the mass function. The masses are primarily sensitive to an accurate determination of M_{bol} , which we expect to be better determined using the bolometric corrections determined from spectral types.

clusters or their spectroscopically derived distance is inconsistent with their being cluster members.

Although our data are consistent with the h/χ stars having formed in a single burst, we cannot rule out other scenarios. For instance, if the primary burst of star formation has occurred at 13 Myr, with a smaller, secondary burst at 10 Myr, we would very likely not discern this in our CMD. There would be few high mass stars, and the lower mass stars would be indistinguishable from their 13 Myr counterparts.

3.4.4. *Stellar Masses, the Mass Function, and Mass Segregation*

Masses are inferred for individual stars by interpolating between the mass tracks on the HR diagram. By counting the number of stars found in each mass bin, we derive the “present day mass function” (PDMF). To the extent that star formation may be coeval, this is equivalent to the initial mass function (IMF) except for the depopulation of the highest mass bin.

In order to minimize the effect of field star contamination, PDMFs have been constructed only for the two regions within 7 arcmin of the cluster cores. In addition, we exclude a few stars found redwards of the main-sequence, and presumed to be foreground contaminants, by eliminating stars in the region constrained between $M_{\text{bol}} < -20.5 \times \log T_{\text{eff}} + 82.5$ and $M_{\text{bol}} > -5$. We used a lower mass cutoff of $4 M_{\odot}$ below which field and pre-main sequence star contamination dominate. At the high-mass end, we expect that evolution through the supernova phase will have depleted stars above $\sim 15 - 20 M_{\odot}$, and so we have used only the mass bins below this to compute the slope of the IMF. We combine all of the higher-mass stars into one mass bin. Following Scalo (1986), we define the quantity ξ as the number of stars per mass bin divided by the difference in the base-ten logarithm of the upper and lower bin masses, and also by the surface area in kpc. The run of $\log \xi$ with \log mass then provides the slope, Γ , of the IMF/PDMF. Values for the number of stars and for ξ are given in Table 3.

Figure 8 shows PDMFs in the 4-16 M_{\odot} range for stars within 7 arcmin of the cluster centers. Error bars are based on $\pm\sqrt{N}$ statistics. We obtain values of $\Gamma = -1.36 \pm 0.20$ for h Per and $\Gamma = -1.25 \pm 0.23$ for χ Per. Within the errors of our fits, both slopes are in good agreement with each other and also with the Salpeter value of $\Gamma = -1.35$. This result can be compared with what is known of the IMF in other young OB associations and clusters, where a weighted average yields $\Gamma = -1.1 \pm 0.1$ for the Milky Way $\Gamma = -1.3 \pm 0.1$ for the LMC/SMC (Massey 1998b). Thus, an IMF slope of $\Gamma = -1.3 \pm 0.2$ for h and χ is in no way

unusual.

Based on extrapolation of the measured PDMFs to $120 \mathcal{M}_\odot$, we estimate that ~ 40 supernovae have occurred in the past in the central regions of the h/ χ Per clusters. Assuming a constant mass function from 1- $120 \mathcal{M}_\odot$, we can estimate the total stellar mass within each of the cluster centers down to $1 \mathcal{M}_\odot$. We find values of $3700 \mathcal{M}_\odot$ and $2800 \mathcal{M}_\odot$ for h Per and χ Per, respectively. This is about 8-10 times that of the mass in $>1 \mathcal{M}_\odot$ stars in the younger Orion Nebula cluster ($\sim 450 \mathcal{M}_\odot$) or the older Pleiades ($\sim 320 \mathcal{M}_\odot$). For comparison, a “supercluster” like R136 in the LMC has a mass of roughly $3 - 4 \times 10^4 \mathcal{M}_\odot$ in $>1 \mathcal{M}_\odot$ stars (Hunter et al. 1996), about a factor of 10 greater than either h or χ and a factor of almost 100 greater than Orion or the Pleiades.

In Figure 9 we explore the evidence for concentration and mass segregation in the two clusters. In doing so, we consider only those stars satisfying our criteria for inclusion in the PDMF. In viewing these panels it should be noted that the 2σ surface density contour in the spatial distribution of stars occurs at radii of ~ 7 arcmin for both h Per and χ Per. The top and middle panels of Fig. 9 show that inside of 7 arcmin, both the mass surface density and the number surface density begin to rise noticeably above the field star surface density, and then steepen considerably at ~ 3 arcmin. The increase in density at smaller cluster radii is evidence of higher central concentration.

The histograms of the total mass/ pc^2 as a function of radial distance (top panels of Fig. 9) show that h Per is about twice as dense at its core compared to χ Per. This occurs both because h Per has $\sim 25\%$ more stars at its center (as can be seen in the middle panels of Fig. 9) and because it contains several high mass ($> 30 \mathcal{M}_\odot$) B supergiants. However, the density profile of h Per falls off more rapidly than that of χ Per and the two clusters are roughly equivalent in mass density at a radius of ~ 3 arcmin.

The bottom panels of Fig. 9 show the average mass as a function of radial distance from the cluster centers. For h Per, we find a significant gradient inside of ~ 7 arcmin in the mean mass *vs.* radial distance, suggestive of mass segregation. The data for χ Per is less convincing, yet we still find the mean stellar mass to be higher by $\sim 1.5 - 2\sigma$ within the central 1 arcmin. This phenomenon has been claimed with varying degrees of strength in other open clusters in the Galaxy (e.g. the Orion Nebula Cluster; Hillenbrand & Hartmann 1998 and references therein) and in the Magellenic Clouds (e.g. R136; Hunter et al 1995, and NGC 1805 and NGC 1818; deGrijs et al 2002). However, unlike their younger counterparts, the mean mass gradient in h/ χ Per may not be primordial, i.e. associated with the formation of the clusters. Assuming a velocity dispersion of $\sigma_v \approx 3$ km/s and a 7 arcmin (4.79 pc) cluster radius, we estimate a crossing time of ~ 1.56 Myr for each of the cluster nuclei. Given that the clusters are ~ 13 Myr old, the age/ $t_{cross} \approx 8$ and hence dynamical relaxation may indeed

play some part in the observed mass segregation.

4. Discussion

4.1. Comments on the Uniqueness of h/χ Per

The h/χ Per clusters are separated by about 30 arcmin on the sky, equal to 20 pc, and are located $\sim 3.5^\circ$ or 140 pc out of the plane of the Galaxy. They are thus similar to but larger and more massive than the younger, closer Orion Nebula cluster and NGC 2024 pair which are separated by ~ 32 pc and located ~ 150 pc out of the plane, or the IC 348 and NGC 1333 pair ~ 21 pc from each other and ~ 122 pc from the plane. As noted above, however, the massive star content of h/χ Per is more than an order of magnitude higher it is in these regions. Other suggested coeval double cluster systems include the older SL 538 / SL 537, SL 353 / SL 349, SL 387 / SL 385, NGC 1971 / NGC 1972, and NGC 1850 pairs (e.g. Dieball & Grebel 1998, 2000a, 2000b and references therein) all in the LMC (see Bhatia & Hatzidimitriou 1988 and Hatzidimitriou & Bhatia 1989 for other LMC and SMC candidates), and the young NGC 206 (van den Bergh, 1966; see also Massey, Armandroff, & Conti 1986) in M31. The range in scale of “double-cluster” formation may extend, therefore, from clusters of individual size ranging from a few pc up to a few hundred pc in diameter. In the younger of these double clusters, for example the ONC / NGC 2024 pair, the stellar and cluster dynamics are still dominated by molecular gas and the clusters are at best only marginally/loosely bound once the gas dissipates, unlike h/χ Per which have survived as bound clusters for ~ 10 Myr after gas dissipation. At present, however, kinematic studies of the h/χ Per cluster motions relative to one another are needed in order to decipher whether the h/χ Per clusters are a true binary system, or merely reflective of synchronized star formation on larger size scales.

Despite the above suggestion that double-cluster formation may be fairly common, we now argue that h/χ Per are nearly unique. They are remarkably similar clusters insofar as we find their distances, reddenings, ages, IMF slopes, and physical sizes to be indistinguishable. The stellar density of h/χ Per, however, is a factor of 2 higher than that of χ Per and its total mass about 1/3 more. Independent of whether this single difference is considered or ignored, the h/χ Per system evokes the word “unique” when considered in the context of the Galaxy. The system is, after all, commonly known as *the* double cluster. While the LMC may contain a high proportion of double clusters that are coeval, these systems show a wide range in total mass ratio and size ratio (see, e.g. Leon, Bergond, & Vallenari (1998)).

4.2. Comments on the Relationship Between h/χ Per and Per OB1

The h/χ Per clusters are often described as the core of the Per OB1 association, located in the Perseus spiral arm at a distance of ~ 2.3 kpc (Humphreys 1978; Ruprecht 1966). A similar relationship between clusters and associations may hold in other cases, such as the pair of open clusters IC 1805/IC 1848 and Cas OB6, seen in projection only 5 degrees from h/χ . Garmany & Stencel (1992) question the physical relation between h/χ Per and the Per OB1 association, other than being located along the same line of sight and in the same spiral arm which is nearly perpendicular to our line of sight in the direction $l \approx 135^\circ$. That we see h/χ Per projected in a field star distribution that is, to within a factor of 30%, at the same distance as the clusters complicates discussion of the cluster / OB association relationship. This discussion is further complicated by the similarity in age between the Per OB1 “field” population and the h/χ Per clusters.

Per OB1 is particularly notable for containing the largest number of red supergiants (RSGs) among the associations whose high-mass members were catalogued (e.g. Blanco 1955; Humphreys 1970; Garmany & Stencel 1992; see also Bidelman 1947b), as well as a substantial number of A- and B-type supergiants (Bidelman 1943). RSGs are visible only for a narrow range of ages between 10-25 Myr at the completeness limit of our photometry and considering the distance to the Perseus spiral arm. Thus it is difficult to reconcile whether the red supergiants at large projected distances from the h/χ Per cluster (black points at $\log T_{\text{eff}} = 3.5$ in the left panel of Fig. 7) are part of the “field” or the result of past ejection from the h/χ Per cluster core regions. Ejection of massive stars from a dense cluster can occur for particular binary and system orbital parameter combinations, but requires that the cluster is mass segregated at very young ages, e.g. at or before the time of gas expulsion. (Kroupa, 2002). Populating the entirety of the Per OB association with stars ejected from the centers of h/χ Per is unlikely, though the effect may be as large as 10-30% by the present cluster ages. The double nature of the cluster may also be important for stellar dynamics considerations.

Along the main sequence of the HR diagram we find reasonable agreement between the cluster and “field” populations again due to the similarity in distance and age of the massive star population. But this does not prove physical association between the clusters and the “field” or association. Even kinematic information would be of limited use in this debate, given the magnitude of the effect compared to achievable errors.

4.3. Future Work

At an age of 13 Myr, the h/ χ Per clusters occupy a particularly interesting age range for investigations of circumstellar disk dissipation and of stellar angular momentum evolution. The evolutionary paths of these phenomena are very poorly understood inbetween the age ranges of well-studied star-forming regions (<1-3 Myr) and the nearest open clusters (IC 2602 and IC 2391 at 50 Myr, α Per at 80 Myr, and the Pleiades at 120 Myr). Despite the larger distance relative to some of these other well-studied open clusters, investigations of the lower-mass (< $3M_{\odot}$) stellar content of h/ χ Per is therefore of great interest. Substantial field star contamination will complicate this issue and require selection techniques such as x-ray or H α emission, or photometric variability, to separate young active candidate cluster members from the Galactic plane foreground/background in a photometric survey.

5. Summary

We have studied the h and χ “double cluster” using modern imaging and spectroscopic techniques. We find that the two clusters have indistinguishable reddenings ($E(B - V) = 0.56$) and distances [$(m - M)_o = 11.85$], values consistent with those cited in the literature. Especially impressive is that these conclusions are identical to those of Wildey (1964), whose data we find holds up extremely well against the current analysis.

Where we differ with previous studies such as Wildey’s (1964) is in our recognition of the significant effect that field star contamination has on the determination of cluster ages. Inclusion of foreground younger stars and GK giants can easily lead to apparent branching in the HR Diagram which has been misinterpreted in the past as an age spread. We find mean ages of 12.8 Myr for each of the two clusters and no evidence for multiple epochs of star formation.

The present day mass function yields a slope consistent with that found in other well-studied Galactic OB associations and clusters ($\Gamma \sim -1.1 \pm 0.1$, see Massey 1998b), and is essentially Salpeter ($\Gamma = -1.35$). In addition, we do find some evidence of mass segregation. The total masses are $3700 M_{\odot}$ for h Per and $2800 M_{\odot}$ for χ Per, for stars with $> 1M_{\odot}$.

6. Acknowledgements

Our interest in h and χ Per traces back to several conversations with Stephen Strom, who remarked at least once how hard it was to understand a 50 Myr age spread, lamenting

that “If we don’t understand star formation in h and χ Per, then where do we understand it?” We hope that we have partially addressed this concern. It is a pleasure to thank Michael Meyer and John Carpenter for work they did in measuring coordinates of the h and χ stars which we used for spectroscopy prior to our CCD imaging efforts. We also acknowledge help and advice from George Jacoby in obtaining the Mosaic data. CLS became involved in this project as a Research Experiences for Undergraduates participant in 1999, and her efforts were supported first by the National Science Foundation (NSF) under grant 99-88007 to Northern Arizona University and more recently by an NSF Graduate Research Fellowship. We dedicate this paper to the memory of Bob Wildey, whose PhD thesis on the subject of h/χ Per should be required reading for all students of Galactic astronomy.

REFERENCES

- Appenzeller, I. 1967, *PASP*, 79, 102
- Balona, L. A. & Shobbrook, R. R. 1984, *MNRAS*, 211, 375
- Balona, L. A. & Feast, M. W. 1975, *MNRAS*, 172, 191
- Bernasconi, P. A. 1996, *A&AS* 120, 57
- Bhatia, R. K. & Hatzidimitriou, D. 1988, *MNRAS*, 230, 215
- Bidelman, W. P. 1943, *ApJ*, 98, 61
- Bidelman, W. P. 1947a, *AJ* 52, 121
- Bidelman, W. P. 1947b, *ApJ* 105, 492
- Blaauw, A. 1964, *ARAA*, 2, 213
- Blanco, V. M. 1955, 122, 434
- Conti, P. S. 1988, in *O Stars and Wolf-Rayet Stars*, ed. P. S. Conti & A. B. Underhill (NASA SP-497)
- Crawford, D. L., Glaspey, J. W., Perry, C. L., 1970, *AJ*, 75, 822
- de Grijs, R., Gilmore, G. F., Johnson, R. A., & Mackey, A. D. 2002, *MNRAS*, 331, 245
- Dieball, A. & Grebel, E. K. 1998, *A&A*, 339, 773
- Dieball, A. & Grebel, E. K. 2000a, *A&A*, 358, 144
- Dieball, A. & Grebel, E. K. 2000b, *A&A*, 358, 897
- FitzGerald, M. P. 1970, *A&A*, 4, 234
- Flower, P. 1996, *ApJ*, 469, 355
- Garmany, C. D. & Stencel, R. E. 1992, *A&AS*, 94, 211
- Hatzidimitriou, D. & Bhatia, R. K. 1990, *A&A*, 2230, 11
- Hillenbrand, L. A. 1997, *AJ*, 113, 1733
- Hillenbrand, L. A. & Hartmann, L. W. 1998, *ApJ*, 492, 540
- Humphreys, R. W. 1970, *ApJ*, 160, 1149
- Humphreys, R. M. 1978, *ApJS*, 38, 309
- Humphreys, R. M., & McElroy, D. B. 1984, *ApJ*, 284, 565
- Hunter, D. A., Shaya, E. J., Holtzman, J. A., Light, R. M., O’Neil, E. J., & Lynds, R. 1995, *ApJ*, 448, 179

- Hunter, D. A., O’Neil, E. J., Lynds, R., Shaya, E. J., Groth, E. J., & Holtzman, J. A. 1996, *ApJ*, 459, L27
- Jacoby, G. H., Hunter, D. A., & Christian, C. A. 1984, *ApJS*, 56, 257
- Jaschek, C. & Jaschek, M. 1987, *The Classification of Stars*, (Cambridge: Cambridge University Press)
- Johnson, H. L. & Morgan, W. W. 1955, 122, 429
- Keller, S. C., Grebel, E. K., Miller, G. J., & Yoss, K. M. 2001, *AJ* 122, 248
- Kilian, J. 1992 *A&A* 262, 171
- Kroupa P., 2002, *Binary Stars, Star Clusters and the Galactic Field Population*, habilitation thesis, University of Kiel.
- Kurucz, R. 1992, in *The Stellar Populations of Galaxies*, ed. B. Barbuy & A. Renzini (Dodrecht: Kluwer), 225
- Landolt, A. U. 1992, *AJ*, 104, 340
- Leon, S., Bergond, G., & Vallenari, A. 1998, *A&A*, 344, 450
- Marco, A. & Bernabeu, G. 2001, *A&A*, 372, 477
- Massey, P. 1998a, in *Stellar Astrophysics for the Local Group*, ed. A. Aparcicio, A. Herrero, & F. Sanchez (Cambridge, Cambridge Univ. Press), 95
- Massey, P. 1998b, in *The Stellar Initial Mass Function*, ed. G. Gilmore & D. Howell (Provo, ASP), 17
- Massey, P., Armandroff, T. E., & Conti, P. S. 1986, *AJ*, 92, 1303
- Massey, P., Johnson, K. E., & DeGioia-Eastwood, K. 1995, *ApJ*, 454, 151
- Massey, P., Waterhouse, E., & DeGioia-Eastwood, K. 2000, *AJ*, 119, 2214
- Morgan, W. W., Code, A. D., & Whitford A. E. 1955, *ApJS*, 2, 41
- Morton, D. C. & Adams, T. F. 1968, *ApJ*, 151, 611
- Oosterhoff, P. Th. 1937 *Ann. Sterrew. Leiden* 17, 1
- Ruprecht, J. 1966, *BAC* 17, 33 and 17, 98 (erratum)
- Scalo, J. M. 1998, *Fundam. Cosmic Phys.*, 11, 1
- Schaller, G., Schaerer, D., Meynet, G., & Maeder, A. 1992, *A&AS*, 96, 269
- Schild, R. 1965, *ApJ*, 142, 979
- Schild, R. 1967, *ApJ*, 148, 449

- Schmidt-Kaler, Th. 1982, in *Astronomy and Astrophysics*, Vol. 2b, Stars and Star Clusters, ed. K. Schaifers & H. H. Voigt (Berlin: Springer), 454
- Slettebak, A. 1968, *ApJ* 154, 933
- Tapia, M., Roth, M., Costero, R., & Navarro, S. 1984, *RMAA*, 9, 65
- Valdes, F. 1998, *Guide to the NOAO Mosaic Data Handling Software*, NOAO Publication.
- Van den Bergh, S. 1966, *AJ*, 71, 219
- Vogt, N. 1971, *A&A*, 11, 359
- Waelkens, C., Lampens, P., Heynderickx, D., Cuypers, J., et al. 1990, *A&AS*, 83, 11
- Walborn, N. R. & Fitzpatrick, E. L. 1990, *PASP*, 102, 379
- Willey, R. L. 1964 *ApJS*, 8, 439

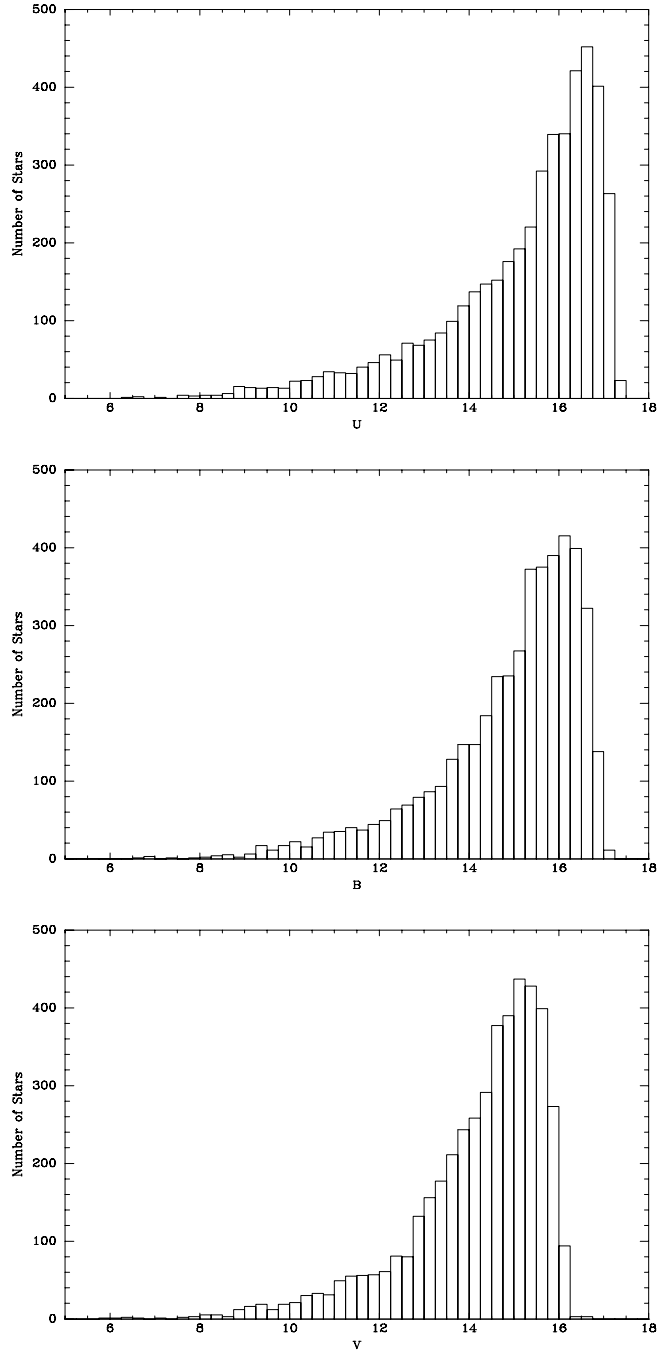


Fig. 1.— For each of our three filters, we use the histogram of the number of stars as a function of magnitude to estimate our completeness.

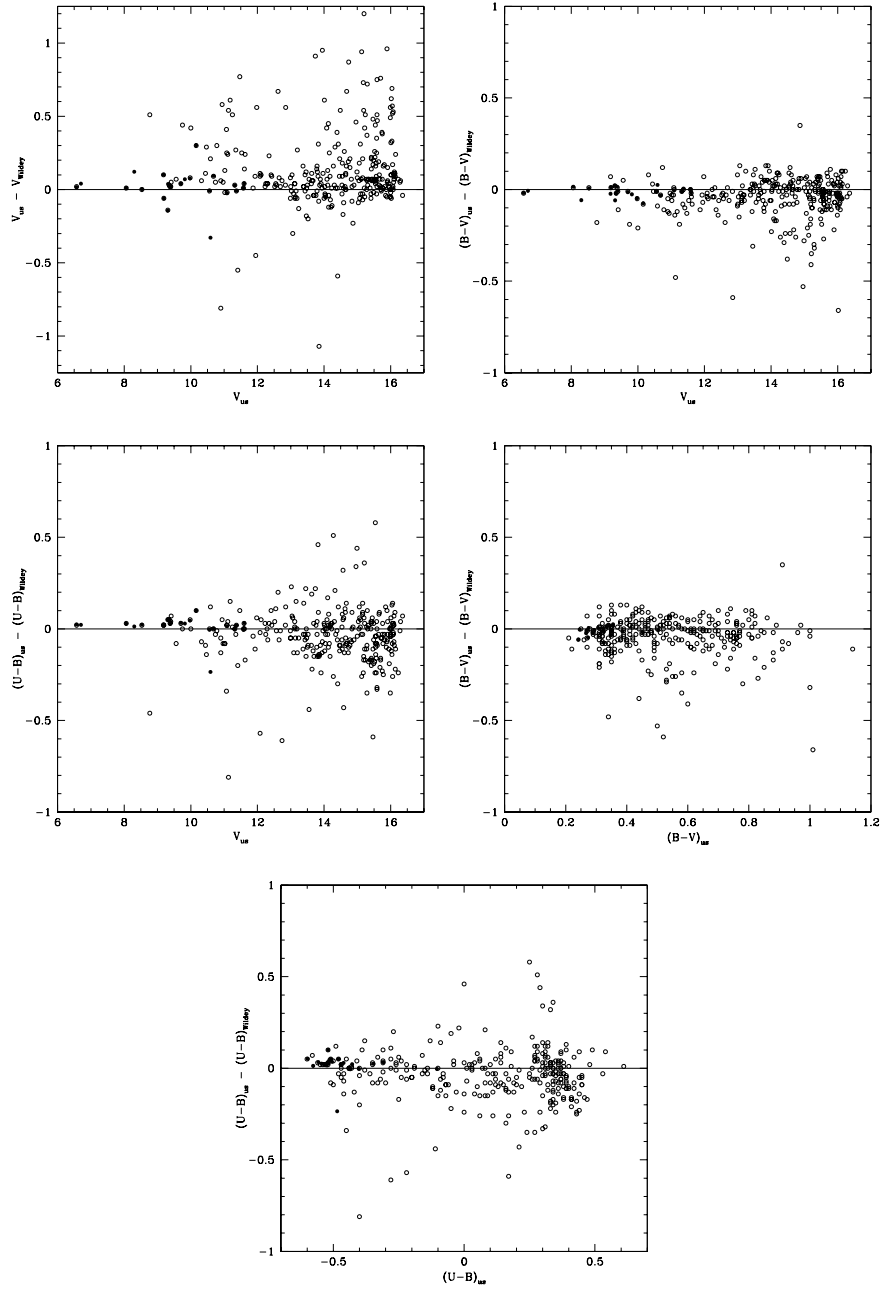


Fig. 2.— Our CCD photometry is found to agree well with that of Wildey’s (1964) data. Open and closed circles are a comparison to his photographic and photoelectric photometry, respectively.

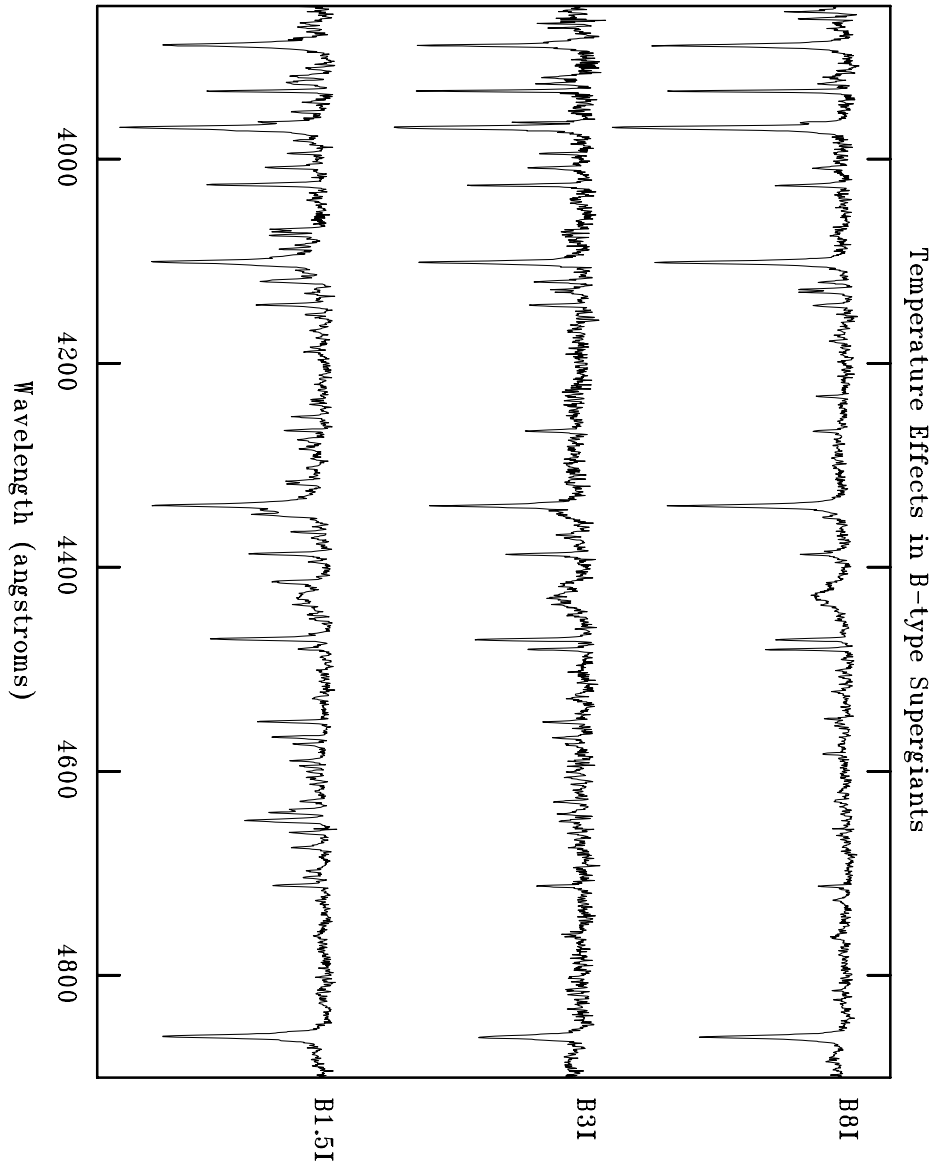


Fig. 3.— Temperature effects in B-type supergiants. The primary indicator is the ratio of MgII 4481 to HeI 4471.

Fig. 4.— THIS FIGURE AVAILABLE IN .GIF FORMAT On the left we show the uncorrected CMD for all of the stars in our sample (upper panel), along with their spatial distribution (lower panel). We have overlaid colored symbols on the stars for which we have spectral types. These may be compared to the diagrams on the right, where we have included only stars within 7 arcmin of the nuclei of the two clusters. Stars near the center of h Per are indicated in blue, while stars near the center of Chi Per are indicated in red.

Fig. 5.— THIS FIGURE AVAILABLE IN .GIF FORMAT The top panels show the full CMDs plotted as contoured Hess diagrams, where we have overlaid color contours to indicate the field-star contamination. In the bottom panels we have removed the field-star contamination and smoothed the data.

Fig. 6.— THIS FIGURE AVAILABLE IN .GIF FORMAT The dereddened CMD for stars within 7 arcminutes of the center of h (blue) and χ (red) Per are shown now with the ZAMS and post-main-sequence isochrones of 10 and 20 Myr indicated. Corresponding 10 and 20 Myr pre-main-sequence isochrones are shown as dashed lines. The black points represent the rest of the stars in our full $0.98^\circ \times 0.98^\circ$ field.

Fig. 7.— THIS FIGURE AVAILABLE IN .GIF FORMAT The HR diagram of h and χ Per are shown. On the left we show all of the data, with filled circles showing the data placed by means of spectroscopy, and open circles being the data for which have only photometry. On the right we show only the stars within a 7 arcminute radius of the center of h (blue dots) and χ (red dots).

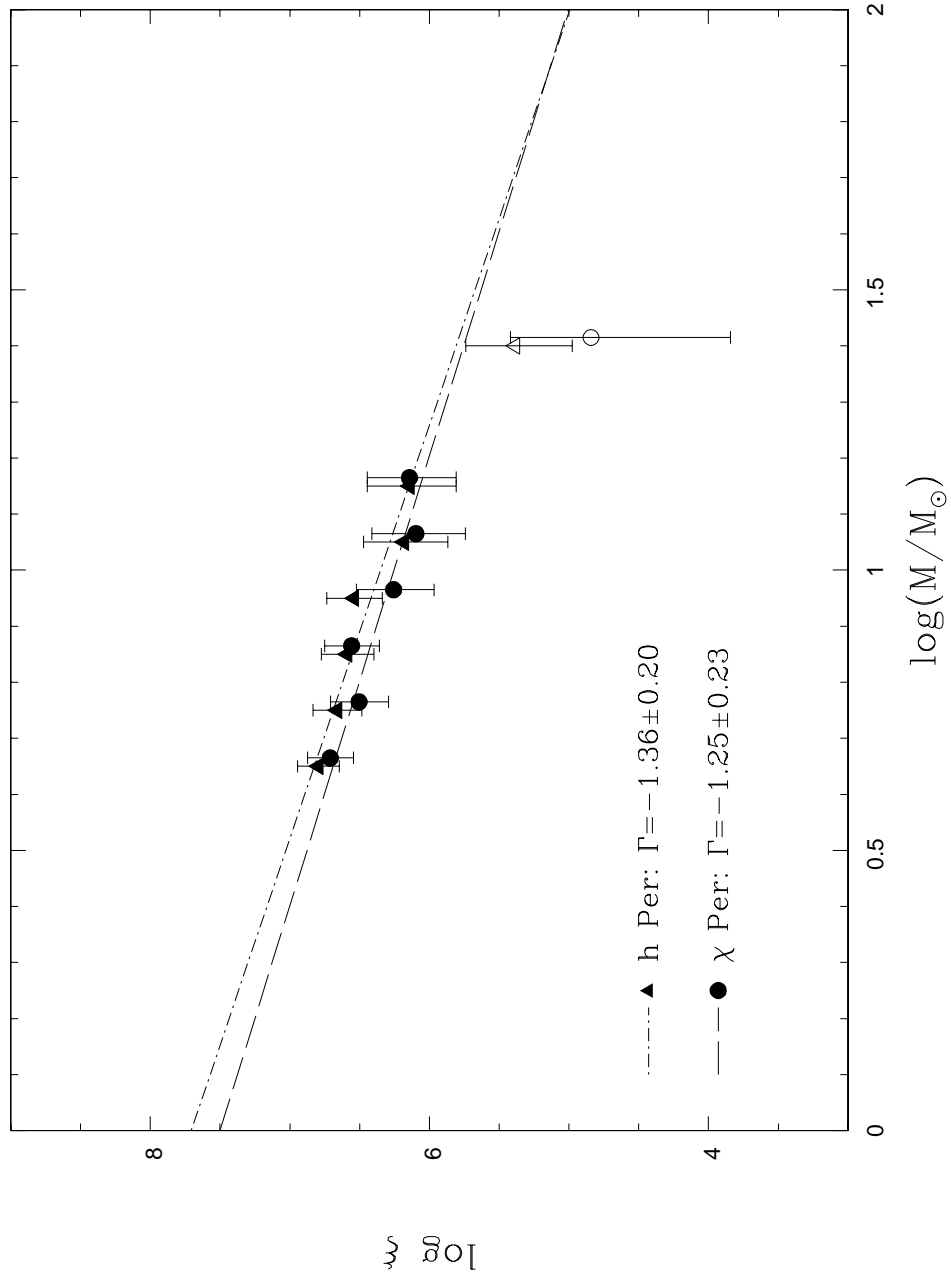


Fig. 8.— The initial mass function is shown for the two clusters. Open symbols indicate an incomplete bin.

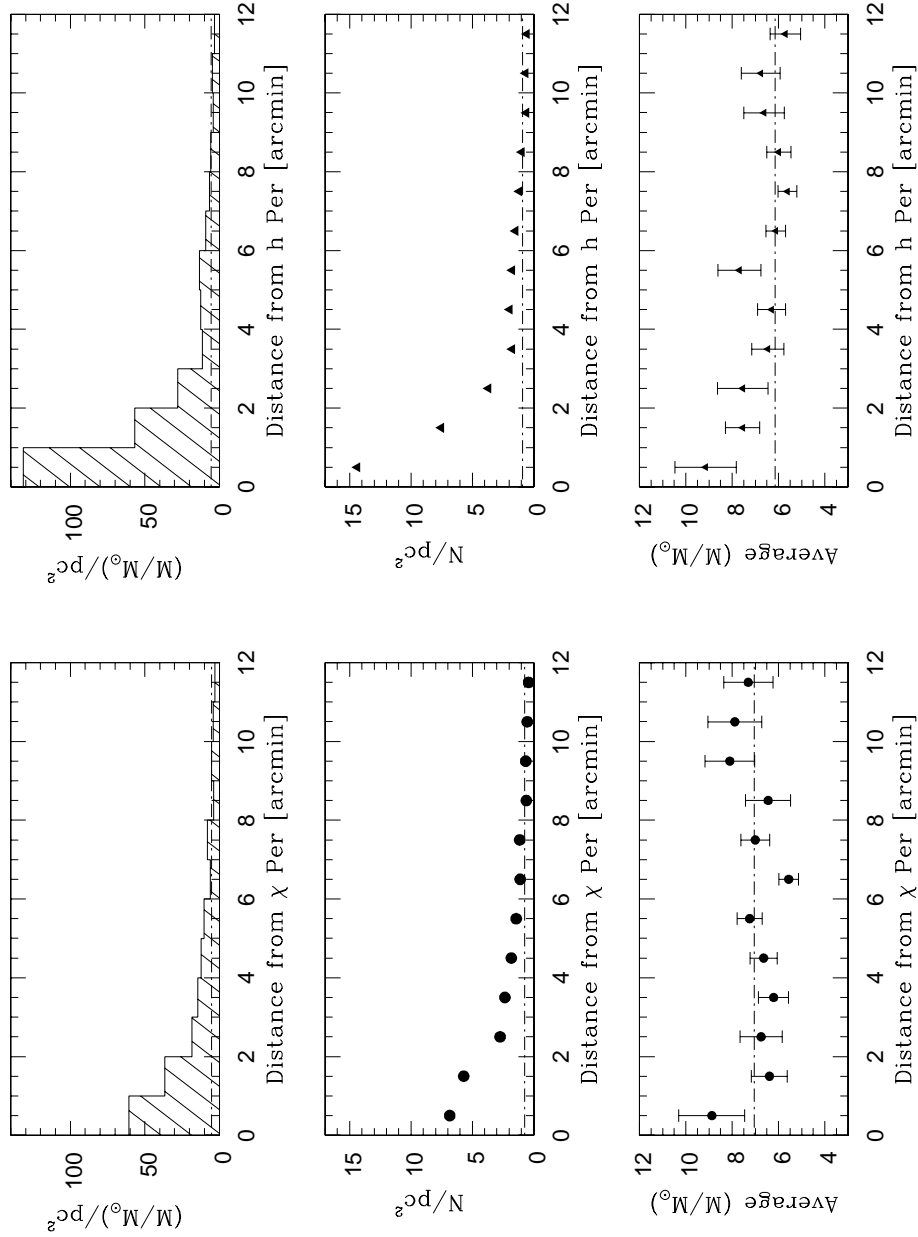


Fig. 9.— The total mass per unit area (top panels), the number of stars per unit area (middle panels), and the average stellar mass per unit area (bottom panels) are shown as a function of radial distance for h Per (left) and χ Per (right). The data have been binned in 1 arcmin rings from the respective cluster centers. Horizontal dashed lines indicate the average of the values from 6-12 arcmin. Within the 2σ surface density enhancements ($r = 7$ arcmin), there is clear evidence in both h and χ Per for central concentration within 3 arcmin (top and middle panels), and also some evidence for mass segregation within 1-2 arcmin (bottom panels).

Table 1. Observational Data^a

ID	α_{2000}	δ_{2000}	V	$(B - V)$	$(U - B)$	d_h^b	d_χ^b	Assoc	Spectral Type		
									Adopted ^c	Literature ^d	Alt. ID ^e
1	2:18:04.44	57:30:58.9	6.023	1.097	0.832	0.389	0.681	far	G7III*	G7III (4)	HD13994
2	2:21:55.32	57:14:34.6	6.480	0.502	-0.050	0.403	0.129	far	A0I	A1Ia (2)	HD14433
3	2:19:04.37	57:08:08.4	6.567	0.452	-0.346	0.016	0.425	h	B3I	B3Ia (1)	HD14134
4	2:19:13.86	57:10:09.8	6.700	0.503	-0.428	0.035	0.405	h	B3I	B2Ia (1)	HD14143
5	2:23:00.35	57:23:13.5	6.977	0.707	-0.249	0.587	0.288	far	B8I	B8Ia (2,3)	HD14542
...
4528	2:19:35.40	57:18:29.9	16.906	0.160	-0.609	0.176	0.400	far

^aThe complete version of this table will be published in the electronic edition.

^bDistances from the cluster centers are given in degrees.

^cA "*" denotes that we have used a spectral type from the literature in our analysis.

^dReferences correspond to: (1) Schild 1965; (2) Johnson & Morgan 1968; (3) Slettebak 1968; (4) Appenzeller 1967; (5) Bidelman 1947b; (6) Morgan, Code, & Whitford 1955.

^eOur cross-identifications are not complete and focus on the brighter stars and those for which we have spectral types. When available, HD or BD numbers are given. All other IDs are taken from Wildey 1964.

Table 2A. Derived Quantities for Probable Cluster Members^a

ID	HRD ^b	$\log T_{eff}$	$E(B - V)$	M_V	M_{bol}	Mass [M_\odot]
3	s	4.300	0.58	-7.09	-9.09	33.1
4	s	4.300	0.63	-7.11	-9.11	33.1
9	s	4.385	0.57	-5.57	-7.99	21.0
12	s	4.370	0.42	-4.86	-7.24	16.4
16	s	4.340	0.56	-5.12	-7.34	16.8
...
1582	p	4.144	0.59	0.59	-0.61	4.0

^aThe complete version of this table will be published in the electronic version.

^bThis column indicates how the star was placed in the HR diagram, with an “s” or “p” meaning using spectra or just photometry, respectively. An “a” indicates that the mean $E(B - V)$ was adopted.

Table 2B. Derived Quantities for Probable Field Stars^a

ID	HRD ^b	$\log T_{eff}$	$E(B - V)$	M_V	M_{bol}	Mass [M_\odot]
1	s	3.680	0.16	-6.31	-6.68	13.7
2	s	4.000	0.50	-6.93	-7.20	16.2
5	s	4.050	0.73	-7.13	-7.71	18.8
6	s	3.940	0.75	-6.73	-6.77	13.9
7	s	3.525	0.62	-5.93	-7.43	13.6
...
1610	p	4.138	0.62	0.52	-0.65	4.0

^aThe complete version of this table will be published in the electronic edition.

^bThis column indicates how the star was placed in the HR diagram, with an “s” or “p” meaning using spectra or just photometry, respectively. An “a” indicates that the mean $E(B - V)$ was adopted.

Table 3. PDMF Data

Mass Range [\mathcal{M}_\odot]	h Per		χ Per	
	N	log ξ	N	log ξ
4.0-5.0	45	6.80	37	6.71
5.0-6.3	33	6.66	23	6.50
6.3-7.9	28	6.59	26	6.56
7.9-10.0	25	6.54	13	6.26
10.0-12.6	11	6.18	9	6.10
12.6-15.8	10	6.14	10	6.14
15.8-40.0	7	5.39	2	4.84

This figure "f4.gif" is available in "gif" format from:

<http://arxiv.org/ps/astro-ph/0205130v1>

This figure "f5.gif" is available in "gif" format from:

<http://arxiv.org/ps/astro-ph/0205130v1>

This figure "f6.gif" is available in "gif" format from:

<http://arxiv.org/ps/astro-ph/0205130v1>

This figure "f7.gif" is available in "gif" format from:

<http://arxiv.org/ps/astro-ph/0205130v1>